Location Independent Vital Sign Monitoring and Gesture Recognition Using Wi-Fi

Chapter · March 2021

DOI: 10.1007/978-3-030-68590-4_7

5 authors, including:

Daqing Zhang
Institut Mines-Télécom
359 PUBLICATIONS **15,916** CITATIONS
SEE PROFILE

Niu Kai
Peking University
22 PUBLICATIONS **311** CITATIONS
SEE PROFILE

Fusang Zhang
Institute of Software, Chinese Academy of Sciences
42 PUBLICATIONS **416** CITATIONS
SEE PROFILE

Shengjie Li
Peking University
14 PUBLICATIONS **726** CITATIONS
SEE PROFILE

Chapter 7
Location Independent Vital Sign Monitoring and Gesture Recognition Using Wi-Fi

Daqing Zhang, Kai Niu, Jie Xiong, Fusang Zhang, and Shengjie Li

Abstract Recent years have witnessed the rapid progress of Wi-Fi based contactless sensing. Compared to traditional wearable based approaches, Wi-Fi sensing does not require the target to wear any sensors and is able to capture rich context information of human target in a non-intrusive manner. Though promising, one major issue hindering the adoption of Wi-Fi sensing is the location and orientation dependence of the performance, i.e., if the human target changes the location or orientation, the sensing performance may degrade significantly. This chapter delves into this issue, analyzes the factors affecting the sensing performance and presents solutions to addressing this issue, moving Wi-Fi sensing one step closer towards real-life deployment.

Keywords Wi-Fi sensing · Unstable performance · Location and orientation dependence · Fresnel Zone model · Virtual multipath · Multiple views

D. Zhang (✉) · K. Niu · S. Li
Peking University, Beijing, China
e-mail: dqzhang@sei.pku.edu.cn

K. Niu
e-mail: xjtunk@pku.edu.cn

S. Li
e-mail: lishengjie@pku.edu.cn

D. Zhang
Telecom SudParis, Institut Polytechnique de Paris, Evry, France

J. Xiong
University of Massachusetts Amherst, Amherst, MA, USA
e-mail: jxiong@cs.umass.edu

F. Zhang
Institute of Software, Chinese Academy of Sciences, Beijing, China
e-mail: zhangfusang@otcaix.iscas.ac.cn

M. A. R. Ahad et al. (eds.), *Contactless Human Activity Analysis*,
Intelligent Systems Reference Library 200,
https://doi.org/10.1007/978-3-030-68590-4_7

7.1 Introduction

Wi-Fi infrastructure is ubiquitously deployed nowadays, which promotes Wi-Fi signals as a promising candidate for contactless human activity sensing. Wi-Fi sensing has enabled a wide variety of applications, ranging from coarse-grained indoor localization [2, 5, 14, 18] and gesture recognition [1, 9, 10, 22] to fine-grained vital sign monitoring [13, 20] and keystroke detection [3]. The basic principle behind Wi-Fi based contactless sensing is that Wi-Fi signals reflected from the human target vary with human activities. Obvious variations can be observed in the Received Signal Strength Indicator (RSSI) or Channel State Information (CSI) retrieved from commodity Wi-Fi devices when human activities occur near the Wi-Fi transceivers. The induced Wi-Fi signal variations can thus be employed to infer the human activities [12, 15]. One key assumption for this to work is that there exists a one-to-one mapping between each human activity and the induced signal variation. This mapping has been verified in constricted settings and a large range of gesture and activity recognition applications have been proposed based on this assumption [1, 4, 16]. However, people soon observed a serious issue related to wireless sensing: the sensing performance is very unstable. While highly accurate sensing can be achieved at one location, the sensing performance can significantly degrade if the target moves even slightly to a nearby location. This issue was theoretically analyzed by Zhang et al. [13, 18, 21] in 2016 and the authors proposed the Fresnel Zone models to characterize the relationship between the signal variations and target movements. It was revealed that the mappings between the human activities and induced signal variations do exist but unfortunately, they are location dependent. That is to say, if the target moves to another location, the mapping changes accordingly, causing performance degradation. It was shown in [13, 20, 21] that just a few centimeters of target displacement can change the sensing performance completely.

In this chapter, we analyze the factors affecting the sensing performance and reveal location and orientation are the key factors affecting the signal variations and accordingly the sensing performance. State-of-the-art solutions proposed to address this location and orientation dependence issue are introduced by employing small-scale human respiration monitoring and large-scale gesture recognition as example applications.

7.2 The Basics of Wi-Fi Sensing

In indoor environment, Wi-Fi signals travel from transmitter to receiver through not only direct line-of-sight (LoS) path but also multipaths. Channel State Information (CSI) is an important physical layer parameter which characterizes the propagation of all these paths in the air. If the transmitted and received signals at carrier frequency f and timestamp t are expressed as $X(f, t)$ and $Y(f, t)$, respectively, the CSI $H(f, t)$ satisfies the equation below:

$$Y(f,t) = H(f,t) \times X(f,t) \tag{7.1}$$

If the Wi-Fi signals arrive at the receiver through M different paths, the overall CSI is the linear superposition of the CSIs of all M paths:

$$H(f,t) = e^{-j\theta_o} \sum_{m=1}^{M} H_m(f,t) = e^{-j\theta_o} \sum_{m=1}^{M} a_m(f,t) e^{-j\cdot(2\pi l_m/\lambda + \theta_r)} \tag{7.2}$$

where $H_m(f,t)$ is the CSI of the mth path, $a_m(f,t)$ is the signal attenuation, $2\pi l_m/\lambda$ is the phase change due to a signal propagation of path length l_m in the air, λ is the signal wavelength, θ_r is the phase change caused by reflection, and θ_o is the random phase shift caused by Sampling Frequency Offset (SFO), Packet Detection Delay (PDD) and Carrier Frequency Offset (CFO) [19].

Consider a typical scenario in Fig. 7.1, there is one pair of Wi-Fi transmitter and receiver. Besides the human target, the wall also reflects Wi-Fi signals. The signal paths can be grouped into two categories: static paths and dynamic paths. The LoS path and the path reflected from the wall are static paths which keep unchanged. The path reflected from the human target is dynamic path as the path length changes with target movement. Without loss of generality, let us assume there is only one dynamic path for easy illustration. As shown in the complex plane in Fig. 7.2, vector

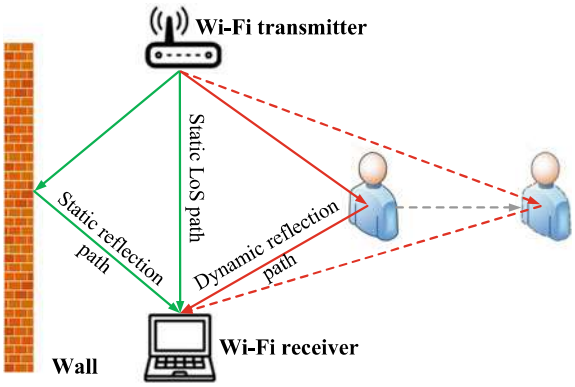

Fig. 7.1 Wi-Fi signals arrive at the receiver through LoS path and reflection paths [7]

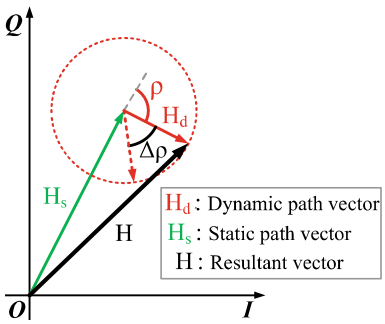

Fig. 7.2 Vector representation of the static and dynamic signals in the I-Q plane: dynamic path vector rotates with respect to the static path vector

H_s represents the sum CSI of the static paths, while vector H_d represents the CSI of the dynamic path. H is the resultant vector which is the sum of the static vector and dynamic vector. The amplitude of H can thus be denoted as:

$$|H|^2 = |H_s|^2 + |H_d|^2 + 2|H_s||H_d|\cos\rho \tag{7.3}$$

where ρ is the phase difference between the static path vector H_s and dynamic path vector H_d. While the static vector[1] does not change, the dynamic vector[2] changes with target movement. However, within a short period of time, the amplitude of the dynamic vector can also be considered as a constant. This is because within a small time window, the displacement due to target movement is in the scale of millimeter or centimeter while the distance between the target and the sensing devices is in the scale of meter. The percentage of the path length change is thus very small and the corresponding amplitude change of the dynamic vector is small enough to be neglected. On the other hand, the phase change of the dynamic vector is large and can not be ignored. Take the 5 GHz Wi-Fi signal as an example, a small target displacement of one centimeter can induce a large phase change of 120°. Therefore, when the target moves slightly from one location to another, the dynamic vector H_d rotates with respect to the static vector H_s as shown in Fig. 7.2. The phase difference change $\Delta\rho$ due to the movement can be calculated as:

$$\Delta\rho = \rho_1 - \rho_0 = 2\pi\,\Delta l/\lambda \tag{7.4}$$

where Δl is the length change of the dynamic path due to target movement. Note that the phase difference change $\Delta\rho$ is the same as the phase change of the dynamic vector because the static vector remains unchanged.

From Eq. 7.3, the signal amplitude $|H|$ is related to three parameters $|H_s|$, $|H_d|$, and ρ. The amplitude of the static vector $|H_s|$ is almost a constant. The amplitude of the dynamic vector $|H_d|$ can also be viewed as a constant in a short time window and thus the phase change of the dynamic vector is the only parameter changing. Two signal variation examples are shown in Fig. 7.3. When the dynamic signal vector rotates, the amplitude of the resultant signal varies like a sinusoidal wave. For one full cycle of 360° phase rotation, a sinusoidal-like wave is obtained with one peak and one valley.

[1]Throughout this chapter, "static path vector", "static signal vector" and "static vector" are used interchangeably.

[2]Throughout this chapter, "dynamic path vector", "dynamic signal vector" and "dynamic vector" are used interchangeably.

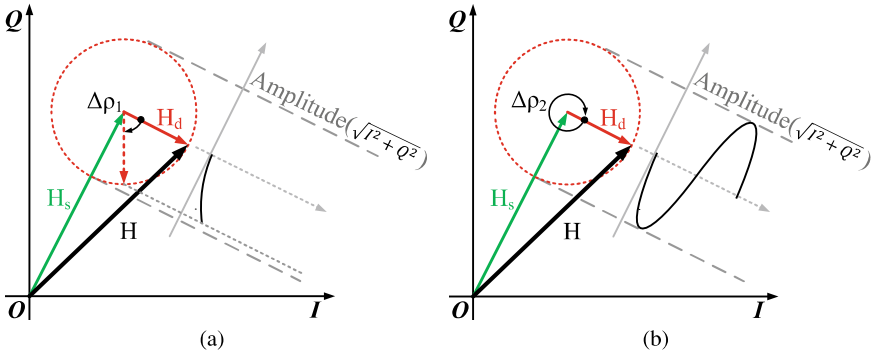

Fig. 7.3 Two signal variation examples: **a** the dynamic signal vector rotates 60° with respect to the static signal vector; and **b** the dynamic signal vector rotates a full cycle of 360° with respect to the static signal vector. The signal amplitude varies like a sinusoidal wave

7.3 Location Dependence Issue in Small-Scale Respiration Sensing

A human respiration cycle contains inhalation and exhalation which expands and contracts lungs respectively, as shown in Fig. 7.4a. The human body can be modeled as a cylinder with slightly varying sizes during respiration. The chest displacement is around 5 mm in the front dimension, 2.5 mm in the back dimension, and 1 mm in the mediolateral dimension [6] during the respiration process, as shown in Fig. 7.4b. For deep respiration, the chest displacement can increase significantly to around 10 mm in the front dimension [8].

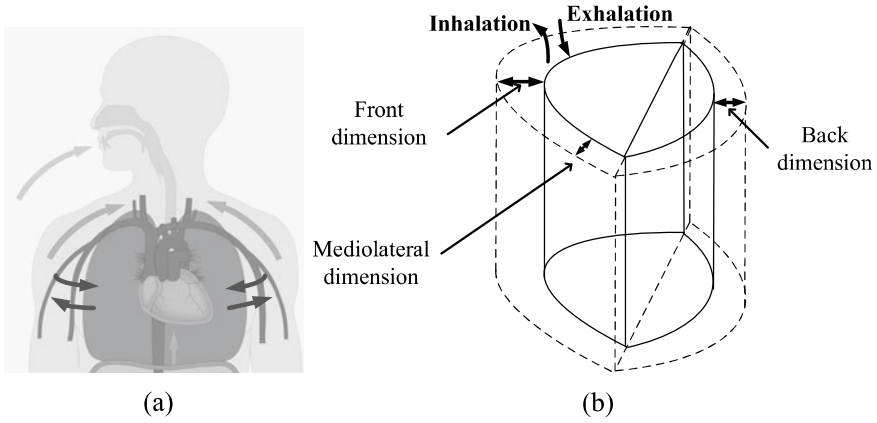

Fig. 7.4 Modeling human respiration: **a** physiological behavior during respiration; and **b** the human body is modeled as a cylinder with varying sizes during respiration

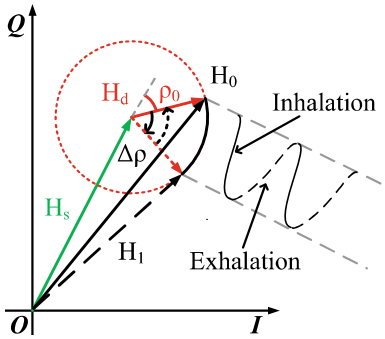

Fig. 7.5 Human respiration induces sinusoidal-like signal amplitude variations

For respiration sensing, the Wi-Fi signals get reflected from the human body such as chest and received at the receiver. The chest displacement causes the reflected signal to vary, and thus, the reflected signal is a dynamic path signal, as shown in Fig. 7.5. Based on the amount of chest displacement, the path length change of the reflected signal can be calculated, which can be further converted into the phase change of the dynamic vector by applying Eq. 7.4. If the chest displacement is Δd_c, the corresponding path length change is roughly $2\Delta d_c$ [11]. For a 5 mm chest displacement, the phase change of the dynamic path signal is 60° for 5 GHz Wi-Fi signals. This phase rotation of 60° induces sinusoidal-like signal amplitude variations as shown in Fig. 7.5. The signal variations in solid and dotted lines correspond to inhalation and exhalation respectively.

7.3.1 *The Factors Affecting the Performance of Respiration Sensing*

Intuitively, a larger signal variation indicates a better sensing performance because a small variation can be easily submerged in noise and becomes undetected. Thus, the performance of respiration sensing is quantitatively related to the signal amplitude variation. The amount of signal amplitude variation during the respiration process can be calculated as:

$$\Delta|H| = |H_1| - |H_0| = \frac{|H_1|^2 - |H_0|^2}{|H_1| + |H_0|} \tag{7.5}$$

where $|H_1|$ and $|H_0|$ are the amplitudes of the resultant signal for inhalation and exhalation, respectively. Placing Eq. 7.3 into 7.5, the signal amplitude variation can be further expressed as:

$$\begin{aligned}\Delta|H| &= \frac{2|H_s||H_d|cos\rho_1 - 2|H_s||H_d|cos\rho_0}{|H_1| + |H_0|} \\ &= \frac{-4|H_s||H_d|sin(\rho_0 + \frac{\Delta\rho}{2})sin\frac{\Delta\rho}{2}}{|H_1| + |H_0|}\end{aligned} \tag{7.6}$$

As the dynamic reflected signal is much weaker than the static signal ($|H_d| \ll |H_s|$), $|H_1| \simeq |H_s|$ and $|H_0| \simeq |H_s|$. Thus, Eq. 7.6 can be approximated as:

$$\Delta|H| \simeq -2|H_d|sin(\rho_0 + \frac{\Delta\rho}{2})sin\frac{\Delta\rho}{2} \tag{7.7}$$

So the sensing performance can be qualitatively characterized by the following equation:

$$\eta = ||H_d|sin(\rho_0 + \frac{\Delta\rho}{2})sin\frac{\Delta\rho}{2}| \tag{7.8}$$

Based on Eq. 7.8, the amount of signal variation is determined by three parameters: (i) the amplitude of the dynamic vector $|H_d|$; (ii) the initial phase difference ρ_0 between the static and dynamic vectors and (iii) the phase difference change $\Delta\rho$. The corresponding interpretations of these three parameters are as follows:

- $|H_d|$ is the amplitude of the dynamic vector. When the target is further away from the Wi-Fi transceiver pair, $|H_d|$ is smaller as the reflected signal needs to propagate a longer distance in the air. A smaller $|H_d|$ corresponds to a smaller signal variation and accordingly a poorer sensing performance. $|H_d|$ remains roughly the same while conducting small-scale activity such as respiration.
- ρ_0 is the initial phase difference between the static vector H_s and dynamic vector H_d. A few centimeters of change in target location can result in a large change of ρ_0, affecting the sensing performance of respiration.
- $\Delta\rho$ is the phase difference change during the respiration process. It is determined by the length change of the dynamic path which is related to the amount of chest displacement. A larger chest displacement induces a larger path length change and thus a larger $\Delta\rho$. For instance, a deep respiration induces a larger $\Delta\rho$ and thus can be more easily detected.

7.3.2 The Effect of Target Location

Based on the analysis in Sect. 7.3.1, a few centimeters of target location change leads to a significant change of the initial phase difference ρ_0, affecting the sensing performance. As shown in Fig. 7.6, a human target is located at four different locations. At Location 1, $\rho_0 = -30°$, the respiration causes a small signal variation. When the target moves to Location 2 with $\rho_0 = 15°$, the same respiration induces a much larger

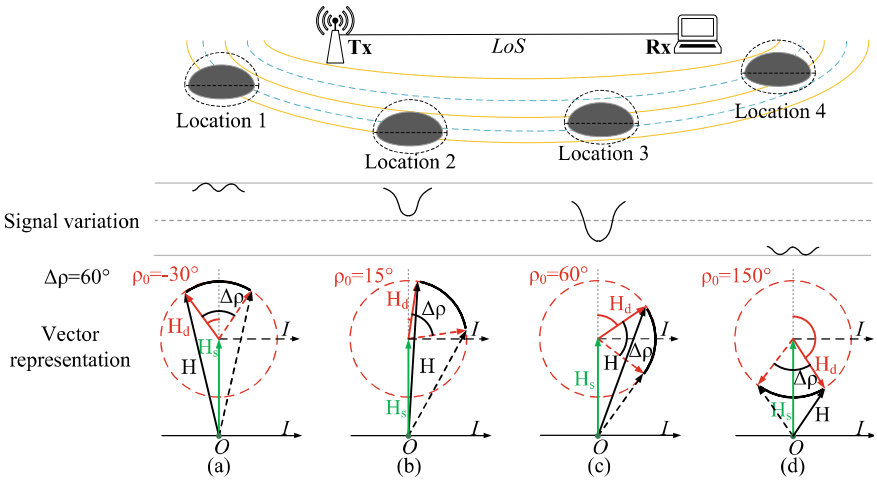

Fig. 7.6 The effect of target location on the performance of respiration sensing

signal variation. At Location 3, $\rho_0 = 60°$, an even larger signal variation is induced. When the target moves further to Location 4 with $\rho_0 = 150°$, a small signal variation is induced and the sensing performance degrades.

7.3.3 The Effect of Target Orientation

During the respiration process, the amount of human body displacement in the front, mediolateral and back dimensions are dramatically different. While the front chest displacement is around 5 mm, the back displacement is only 2–3 mm. Hence, the amount of signal variation changes with the target orientation with respect to the Wi-Fi transceiver pair.

As shown in Fig. 7.7, the target is located at three different locations with similar sensing performance when the target faces the LoS. However, when the target changes the orientation, the sensing performance varies differently. Specifically, when the target chest is facing the LoS at Orientation 1, the largest signal variation can be achieved. At Orientation 2 with the mediolateral dimension facing the LoS, the smallest signal variation is induced. When the target back is facing the LoS at Orientation 3, the body displacement in the back dimension is captured which is smaller than that in the front dimension but still larger than that in the mediolateral dimension.

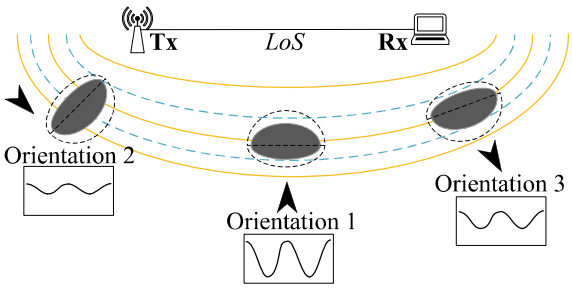

Fig. 7.7 The effect of body orientation on the performance of respiration sensing

7.4 Location Dependence Issue in Large-Scale Activity Sensing

Different from small-scale chest displacement during respiration, the displacement for large-scale human activity is often in the scale of decimeter which induces a much larger path length change. For respiration sensing, the phase rotation is less than one cycle and the sensing performance is only related to the amount of signal variation. For large-scale activities, the phase rotation can span multiple cycles and the minor signal variation is not that important any more. The more important features in differentiating these activities are the number of peaks/valleys and the intervals between them. These features are the focus when dealing with large-scale activity sensing. In this section, the factors affecting these features in large-scale activity sensing are analyzed.

7.4.1 The Factors Affecting Large-Scale Activity Sensing

As shown in Fig. 7.8, when the target moves from location P_1 to P_2, the movement distance Δd can be decomposed into the radial direction component and tangential direction component. Note that if a target moves along the tangential direction, the path length does not change. Thus, only the radial direction component can induce path length change. To quantify the relationship between the target displacement and the path length change, a coefficient r is defined. When the target is far away from the sensing devices, one unit distance of displacement can induce a path length change of two units and thus $r = 2$. The value of r decreases when the target moves closer to the sensing devices. Therefore, the path length change Δl can be denoted as:

$$\Delta l = r \cdot \Delta d \cdot sin\beta \tag{7.9}$$

where Δd is the target displacement, and β is the motion direction with respect to the tangential direction. By placing Eq. 7.9 into 7.4, the phase difference change induced by a large-scale activity can be expressed as:

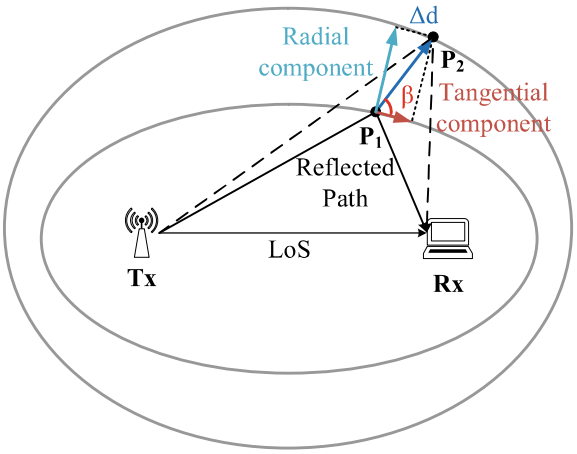

Fig. 7.8 The relationship between target movement distance and reflection path length change

$$\Delta\rho = 2\pi \cdot r \cdot \Delta d \cdot sin\beta/\lambda \tag{7.10}$$

From Eq. 7.10, the phase difference change for a large-scale activity is related to three parameters: (i) the target movement distance Δd, (ii) the coefficient r and (iii) the motion direction β. The corresponding interpretations of these three parameters are as follows:

- Δd is the distance of target movement. Apparently, a larger Δd induces a larger phase change, leading to more cycles of signal variation.
- The coefficient r is dependent on the target location. Fig. 7.9 presents the r values when the target is located at different locations. When the target is far away from the transceiver pair, r is larger and can be approximated as 2. For the same amount of movement distance, a further away target induces a larger signal path length change.
- β is the direction of the target movement. For the same amount of movement distance, if the target moves along the radial direction, $sin\beta = 1$ and the largest number of signal vibration cycles are induced. In contrast, if the target moves along the tangential direction, $sin\beta = 0$ and a minimum number of signal variation cycles are induced.

7.4.2 The Effect of Target Location

For large-scale activities, when the target is at different locations, not just the amplitude of the signal variations is different, the number of signal variation cycles is also different, violating the one-to-one mapping between human activity and induced signal variation. As shown in Fig. 7.10, for the same movement distance, if the target is located at Location 1, 7.5 cycles of signal variation can be observed. When the target

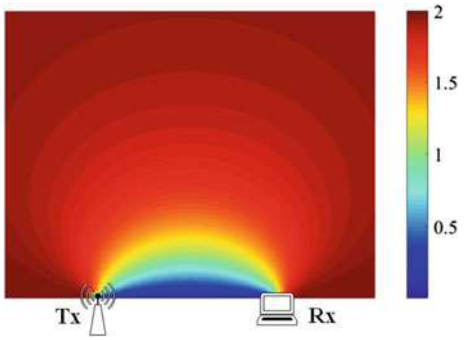

Fig. 7.9 The heatmap for the value of coefficient r at different target locations with respect to the transceiver pair

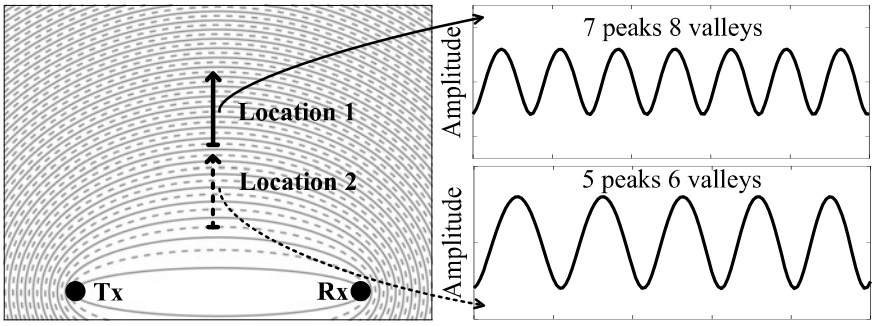

Fig. 7.10 The effect of target location on signal variations for large-scale activities

is closer to the transceiver pair at Location 2, only 5.5 cycles of signal variation can be observed. Of course, the signal variation amplitude is also different. When the target is further away, a smaller variation is induced due to signal power loss.

7.4.3 The Effect of Motion Orientation

Besides location, the motion orientation also affects the number of signal variation cycles. As shown in Fig. 7.11, when the target moves the same distance at different directions, the number of signal variation cycles is dramatically different. At 90° direction, 9 signal variation cycles can be observed. When the target moves at the direction of 45°, only 6.5 cycles are induced. If the target moves at the direction of 0°, only 1.5 cycles are observed.

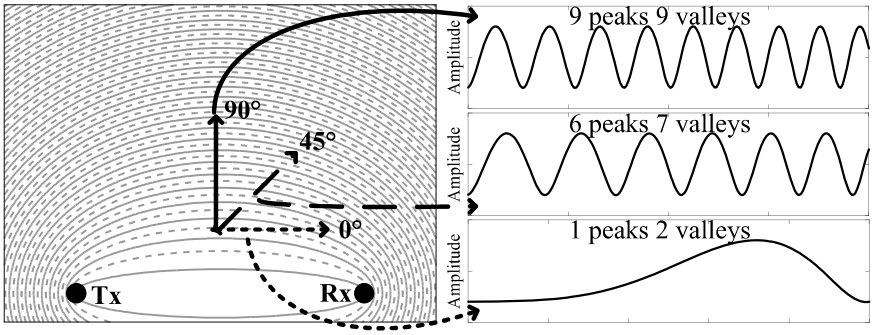

Fig. 7.11 The effect of motion orientation on signal variations for large-scale activities

7.5 Improving the Performance of Respiration Sensing with Virtual Multipath

As introduced in Sect. 7.3, the performance of respiration sensing is dependent on the target location and orientation. At some locations, the performance can be poor and these locations are called "blind spots" in literature [7]. To address this issue, virtual multipath is introduced to improve the performance of human respiration sensing.

Based on the analysis in Sect. 7.3.1, the initial phase difference ρ_0 between the dynamic vector and static vector is the key parameter affecting the performance of respiration sensing. The value of ρ_0 depends on the location of the target with respect to the Wi-Fi transceiver pair. A straightforward method to improve the sensing performance is to change the physical location of the target. However, this is not only inconvenient but also intrusive. Changing the location by a precise amount is also difficult to achieve in practice. It is highly possible the target may need to move multiple times before a satisfactory sensing performance can be achieved. Niu et al. proposed to inject a "virtual" multipath to tune the initial phase difference ρ_0 without requiring the target to physically move [7]. By injecting a carefully designed virtual multipath to change the static vector, the phase difference between the new static vector and dynamic vector can be tuned close to 90° to maximize the signal variation for best sensing performance. As shown in Fig. 7.12, after introducing a static multipath vector H_m, the original static vector H_s is added with the injected multipath vector to form a new static vector H_{snew}. The dynamic vector now rotates with respect to the new static vector H_{snew} as shown in Fig. 7.12b during the respiration process. After the virtual multipath is injected, the initial phase difference ρ_0 becomes ρ_0'. Therefore, the key is to carefully design a multipath to tune the value of ρ_0' close to 90° for best sensing performance [7]. Note that the phase of the dynamic vector keeps changing and thus the best performance is achieved when the phase difference between the static vector and the middle point of the dynamic vector during

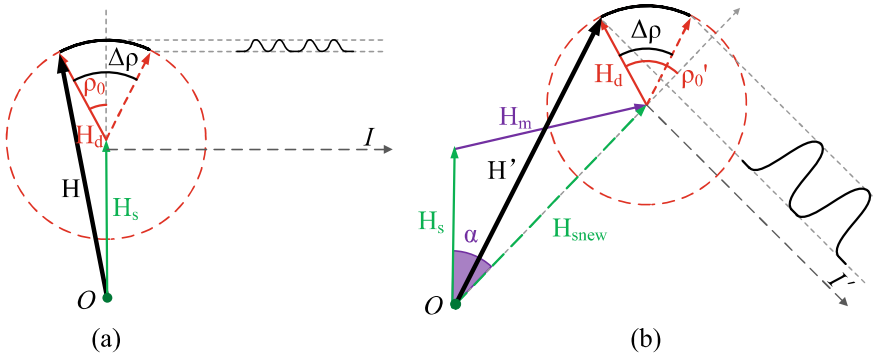

Fig. 7.12 The effect of adding a virtual multipath [7]: **a** small signal variations are induced; and **b** much larger signal variations are induced with a virtual multipath added

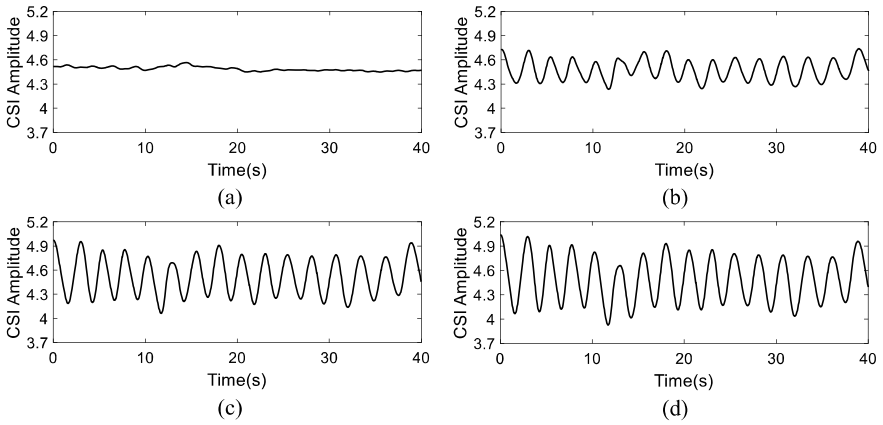

Fig. 7.13 The effect of different virtual multipaths on respiration sensing [7]: **a** original signal variation without multipath; **b** signal variation after adding Virtual Multipath 1; **c** signal variation after adding Virtual Multipath 2; and **d** signal variation after adding Virtual Multipath 3

the movement process is 90°. For simplicity and easy illustration, we just employ the phase difference between the static vector and the initial dynamic vector to explain the concept.

To demonstrate the effectiveness of the virtual multipath approach, the software-defined radio platform WARP [17] is employed as the Wi-Fi transceivers to sense human respiration. The transmitter and receiver are placed at the same height with a distance of one meter between them. The transmitter sends out Wi-Fi signals in the 5.24 GHz frequency band using a 40 MHz channel. Figure 7.13a shows the original signal variation for respiration at a "blind spot". The original signal has a small variation and the periodic respiration pattern can hardly be visualized. Figure 7.13b–d show the new signal variations after three different virtual multipaths are added. The much larger signal variations obtained demonstrate the effectiveness of employing

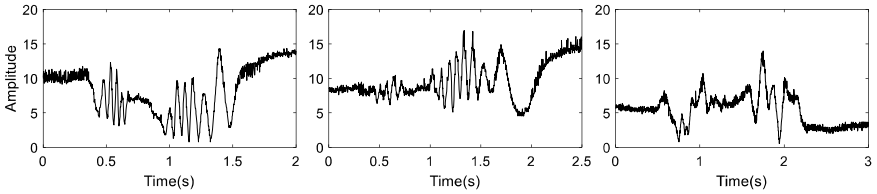

Fig. 7.14 The recorded signal variations for the hand gesture "up-down" in three cases: **a** at position 1 and orientation 90°; **b** at position 2 and orientation 90°; and **c** at position 1 and orientation 0°

virtual multipath to improve the performance of respiration sensing. Among the three virtual multipaths added, Virtual Multipath 3 achieves the best performance by tuning the value of ρ_0' to 90°. Thus, a virtual multipath can be used to address the location dependence issue in respiration sensing and achieve robust performance.

7.6 Applying Multiple Views to Achieve Location Independent Gesture Recognition

In this section, we introduce the concept of multiple views to address the location dependence issue in large-scale gesture recognition. For Wi-Fi sensing, the reflected signals from the target can be received at multiple receivers and these signals can be considered as information from multiple views. We employ gesture recognition as an example to illustrate how to extract features from multiple views to address the location dependence issue in Wi-Fi sensing.

Gesture recognition plays an important role in human-computer interaction and has become one of the most popular applications in wireless sensing. However, a critical issue in Wi-Fi based gesture recognition is that the performance is very unstable. If the target changes the location, the signal variation pattern changes accordingly, breaking the one-to-one mapping between gestures and signal variation patterns. As shown in Fig. 7.14, the same gesture performed at different locations could lead to dramatically different signal variation patterns. The orientation also affects the signal variation pattern, making this issue even more complicated.

Interestingly, though movement induced signal variations are different when the target is at different locations or moves at different orientations, it is observed that the relative movement is independent of location or orientation. For example, one target can face any orientation and then "turn right". The absolute movement directions are different when the target faces different orientations. However, the relative movement direction is always "turn right", which is the same no matter which orientation the target is facing. Thus, the same concept can be applied here and the relative motion direction change can be employed as a location/orientation independent feature for gesture recognition.

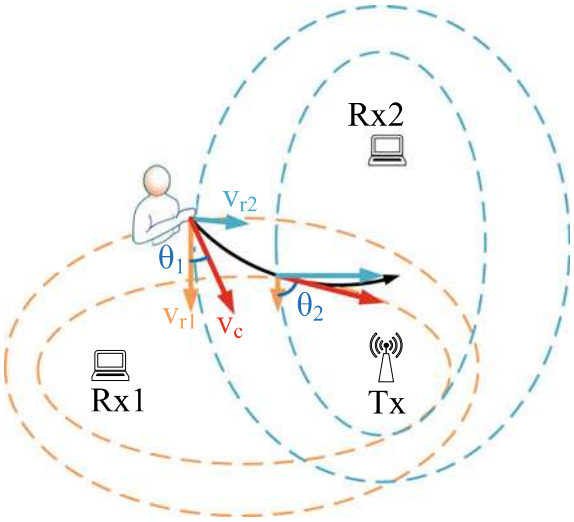

Fig. 7.15 Multi-view concept: different velocity components can be obtained at two receivers to recover the true target velocity

Specifically, the target motion can be characterized by target velocity and the velocity information can be calculated from the Doppler frequency shift. However, the velocity obtained from the Doppler shift is just the radial velocity component, because the tangential velocity component does not change the length of the reflection path. Thus, with one receiver, it is impossible to obtain the target velocity. By including a second receiver and placing it at a carefully chosen location, this problem can be solved because the missing tangential velocity component at the first receiver can be obtained from the second receiver. Thus, signals collected from two views are employed to extract features for sensing. Once the target velocity is obtained, the motion direction change can be calculated and employed to recognize gestures and this motion direction change feature is independent of target location and orientation.

As shown in Fig. 7.15, let us assume the radial velocity component for Receiver 1 is v_{r1} and the radial velocity component for Receiver 2 is v_{r2}. The two receivers are carefully deployed to make sure the two velocity components v_{r1} and v_{r2} are roughly perpendicular to each other. With this setting, the actual target movement direction can be obtained as $\tilde{\theta} = \arctan(v_{r1}/v_{r2})$. For a gesture with a displacement of tens of centimeters, this perpendicular relationship can be assumed to be true throughout the process. The relative change of the motion direction is a feature independent of target location and orientation. Figure 7.16 shows the velocities obtained at two receivers and the relative change of motion direction for the gesture of handwriting a "7" in the air when the target faces two different orientations. We employ the normalized Dynamic Time Warping (DTW) distance to characterize the similarity between two data samples. The similarity value is between 0 and 1 with 1 representing two exactly

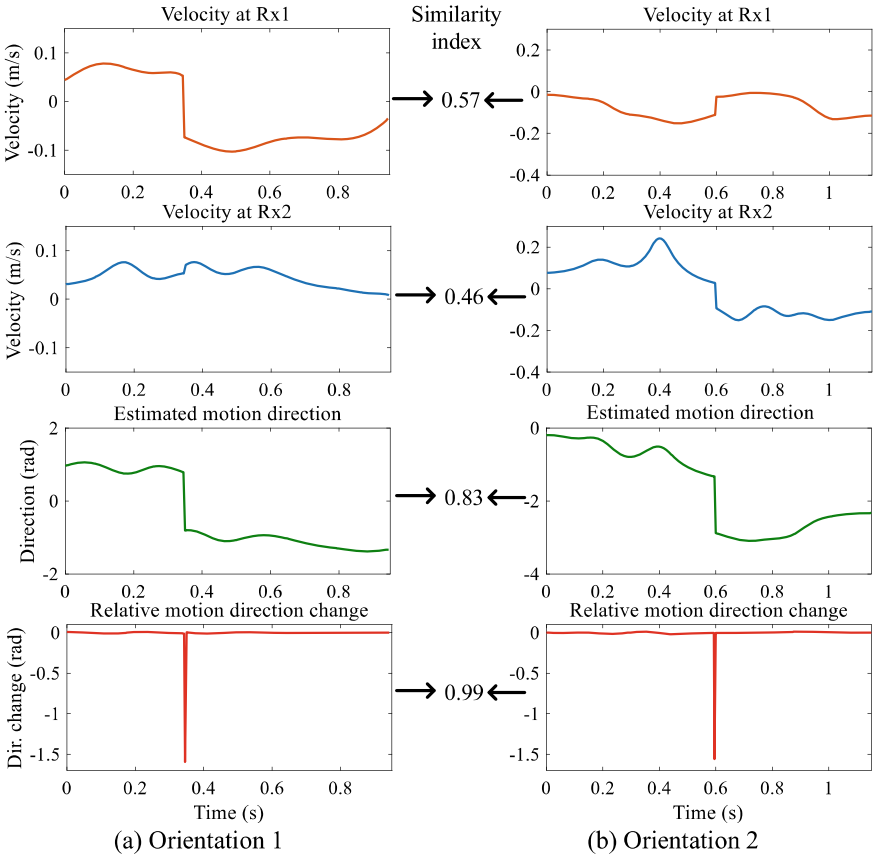

Fig. 7.16 Velocities at two receivers, estimated motion direction, and relative motion direction change when hand-writing "7" in the air at two different orientations

the same inputs. It can be seen in Fig. 7.16 that although the velocity patterns are dramatically different, the relative motion direction changes are very similar with a similarity index of 0.99, independent of gesture orientation.

7.7 Conclusion

In this chapter, we present one critical issue in wireless sensing: the sensing performance is highly dependent on target location and orientation. Through theoretical analysis and benchmark experiments, factors affecting the sensing performance are identified. For small-scale human respiration sensing, virtual multipath is introduced to address the location dependence issue and improve the robustness of respiration

monitoring. For large-scale gesture recognition, the multi-view concept is introduced to obtain a feature independent of target location and orientation, achieving one-to-one mapping between gestures and signal features. We believe the solutions introduced in this chapter are general enough to be applied to other sensing applications using RF signals.

References

1. Abdelnasser, H., Youssef, M., Harras, K.A.: Wigest: a ubiquitous wifi-based gesture recognition system. In: 2015 IEEE Conference on Computer Communications (INFOCOM), pp. 1472–1480 (2015)
2. Adib, F., Katabi, D.: See through walls with wifi!. SIGCOMM Comput. Commun. Rev. **43**(4), 75–86 (2013). August
3. Ali, K., Liu, A.X., Wang, W., Shahzad, M.: Keystroke recognition using wifi signals. In: Proceedings of the 21st Annual International Conference on Mobile Computing and Networking, MobiCom '15, pp. 90–102. ACM, New York, NY, USA (2015)
4. He, W., Wu, K., Zou, Y., Ming, Z.: Wig: Wifi-based gesture recognition system. In: 2015 24th International Conference on Computer Communication and Networks (ICCCN), pp. 1–7 (2015)
5. Li, X., Li, S., Zhang, D., Xiong, J., Wang, Y., Mei, H.: Dynamic-music: accurate device-free indoor localization. In: Proceedings of the 2016 ACM International Joint Conference on Pervasive and Ubiquitous Computing, UbiComp '16, pp. 196–207. ACM, New York, NY, USA (2016)
6. Lowanichkiattikul, C., Dhanachai, M., Sitathanee, C., Khachonkham, S., Khaothong, P.: Impact of chest wall motion caused by respiration in adjuvant radiotherapy for postoperative breast cancer patients. Springer Plus **5**(1), 144 (2016)
7. Niu, K., Zhang, F., Xiong, J., Li, X., Yi, E., Zhang, D.: Boosting fine-grained activity sensing by embracing wireless multipath effects. In: Proceedings of the 14th International Conference on Emerging Networking EXperiments and Technologies, CoNEXT '18, pp. 139–151. Association for Computing Machinery, New York, NY, USA (2018)
8. Pedersen, A., Korreman, S., Nyström, H., Specht, L.: Breathing adapted radiotherapy of breast cancer: reduction of cardiac and pulmonary doses using voluntary inspiration breath-hold. Radiother. Oncol. **72**(1), 53–60 (2004)
9. Pu, Q., Gupta, S., Gollakota, S., Patel, S.: Whole-home gesture recognition using wireless signals. In: Proceedings of the 19th Annual International Conference on Mobile Computing and Networking, MobiCom '13, pp. 27–38. ACM, New York, NY, USA (2013)
10. Sun, L., Sen, S., Koutsonikolas, D., Kim, K.: Widraw: enabling hands-free drawing in the air on commodity wifi devices. In: Proceedings of the 21st Annual International Conference on Mobile Computing and Networking, MobiCom '15, pp. 77–89. Association for Computing Machinery, New York, NY, USA (2015)
11. Wang, W., Liu, X.A., Shahzad, M., Ling, K., Lu, S.: Understanding and modeling of wifi signal based human activity recognition. In: Proceedings of the 21st Annual International Conference on Mobile Computing and Networking, MobiCom '15, pp. 65–76. ACM, New York, NY, USA (2015)
12. Wang, W., Liu, A.X., Shahzad, M.: Gait recognition using wifi signals. In: Proceedings of the 2016 ACM International Joint Conference on Pervasive and Ubiquitous Computing, UbiComp '16, pp. 363–373. ACM, New York, NY, USA (2016)
13. Wang, H., Zhang, D., Ma, J., Wang, Y., Wu, D., Gu, T., Xie, B.: Human respiration detection with commodity wifi devices: Do user location and body orientation matter? In: Proceedings of the 2016 ACM International Joint Conference on Pervasive and Ubiquitous Computing, UbiComp '16, pp. 25–36. ACM, New York, NY, USA (2016)

14. Wang, H., Zhang, D., Niu, K., Lv, Q., Liu, Y., Wu, D., Gao, R., Xie, B.: Mfdl: a multicarrier fresnel penetration model based device-free localization system leveraging commodity wi-fi cards. arXiv:1707.07514 (2017)
15. Wang, H., Zhang, D., Wang, Y., Ma, J., Wang, Y., Li, S.: Rt-fall: a real-time and contactless fall detection system with commodity wifi devices. IEEE Trans. Mobile Comput. **16**(2), 511–526 (2017). Feb
16. Wang, Y., Wu, K., Ni, L.M.: Wifall: device-free fall detection by wireless networks. IEEE Trans. Mobile Comput. **16**(2), 581–594 (2017)
17. Warp project. https://warpproject.org (2017). Accessed 1 Oct 2017
18. Wu, D., Zhang, D., Xu, C., Wang, Y., Wang, H.: Widir: walking direction estimation using wireless signals. In: Proceedings of the 2016 ACM International Joint Conference on Pervasive and Ubiquitous Computing, UbiComp '16, pp. 351–362. ACM, New York, NY, USA (2016)
19. Xie, Y., Li, Z., Li, M.: Precise power delay profiling with commodity wifi. In: Proceedings of the 21st Annual International Conference on Mobile Computing and Networking, MobiCom '15, pp. 53–64. ACM, New York, NY, USA (2015)
20. Zhang, F., Zhang, D., Xiong, J., Wang, H., Niu, K., Jin, B., Wang, Y.: From fresnel diffraction model to fine-grained human respiration sensing with commodity wi-fi devices. Proc. ACM Interact. Mob. Wearable Ubiquitous Technol. **2**(1):53:1–53:23 (2018)
21. Zhang, D., Wang, H., Wu, D.: Toward centimeter-scale human activity sensing with wi-fi signals. Computer **50**(1), 48–57 (2017). Jan
22. Zheng, Y., Zhang, Y., Qian, K., Zhang, G., Liu, Y., Wu, C., Yang, Z.: Zero-effort cross-domain gesture recognition with wi-fi. In: Proceedings of the 17th Annual International Conference on Mobile Systems, Applications, and Services, MobiSys '19, pp. 313–325. Association for Computing Machinery, New York, NY, USA (2019)